Ann. Geophys., 28, 1749–1759, 2010
www.ann-geophys.net/28/1749/2010/
doi:10.5194/angeo-28-1749-2010

Annales Geophysicae

Ray tracing analysis of L mode pumping of the ionosphere, with implications for the magnetic zenith effect

E. Nordblad and T. B. Leyser

Swedish Institute of Space Physics, P.O. Box 537, 751 21 Uppsala, Sweden

Received: 30 March 2010 – Revised: 2 July 2010 – Accepted: 7 September 2010 – Published: 28 September 2010

Abstract. Using ray tracing of ordinary mode HF waves in an ionosphere with kilometre-scale field aligned density depletions, or ducts, we find that transmission across the plasma resonance becomes possible at new locations as rays are guided into the so-called L mode. Stronger transmitted fields are seen in some directions, notably at inclinations close to the vertical or the magnetic zenith (MZ). It is argued that the results could have implications for the magnetic zenith effect, i.e., the increased plasma response that has been observed around the MZ.

Keywords. Ionosphere (Active experiments; Ionospheric irregularities; Wave propagation)

1 Introduction

In ground based high frequency pumping experiments at high altitudes, absorption of ordinary (O) mode pump waves energises the ionospheric plasma and leads to optical emissions, among other effects. The emissions sometimes feature brighter and darker patches, one or a few kilometres wide (Kosch et al., 2007). This suggests the presence of kilometre-scale plasma density perturbations, such as the field aligned density depletions that have been shown to exist by comparing satellite measurements of the plasma density with radar plasma line fluctuations (Farley et al., 1983).

In the present study, we use ray tracing to study how field aligned regions of lower density, referred to as ducts, in an otherwise plane stratified ionosphere affect the propagation of the pump beam. Our results show that refraction at the duct walls not only causes focussing of the beam, but also influences its polarisation and even introduces new points of transmission across the plasma resonance. These results could help explaining optical emissions from altitudes above the O mode reflection height, i.e., the altitude where the plasma frequency, ω_p, equals the pump wave frequency, ω (the plasma resonance). Such effects were reported by Kosch et al. (2004), who observed an annular optical structure extending above the reflection height shortly after the onset of pumping. While at a later stage, the emissions collapsed into a blob at lower altitude and were attributed to Langmuir turbulence, this initial annulus could be due to upper hybrid (UH) waves trapped inside small scale density striations, as we argued in Leyser and Nordblad (2009).

The process of transmission to high altitudes can be understood in terms of L mode (L for left-handed polarisation) electromagnetic waves. Key features of L mode waves are (1) they are associated with radio windows enabling them to pass through the plasma resonance, and (2) they have perpendicular polarisation, i.e., the wave electric field $\boldsymbol{E}$ is perpendicular to the ambient magnetic field $\boldsymbol{B_0}$. The second property means that rays propagating in the L mode can energise the ionosphere efficiently by exciting UH oscillations inside striations (Dysthe et al., 1982). Since L mode propagation thus facilitates conversion into UH waves, it could be important also below the reflection height and in situations where transmission is not relevant. In particular, L mode waves propagating in density ducts can reach the UH resonance in cases where they would otherwise have changed polarisation or been reflected at a much lower altitude.

In a plane stratified ionosphere, radio windows and L mode rays are found only at specific inclinations (Mjølhus, 1990). By guiding O mode waves into the L mode, however, kilometre-scale density depletions open up radio windows also in other directions. There are indications that this mechanism is particularly efficient close to the magnetic zenith (MZ). This fact could potentially help explaining the so-called MZ effect, which refers to observations of increased plasma response around the MZ (Rietveld et al., 2003). Preliminary results pointing in this direction were presented by

Correspondence to: E. Nordblad
(eno@irfu.se)

Leyser and Nordblad (2009). The present study offers a more detailed analysis.

The outline of the paper is the following: after summarising the physics of L mode waves and radio windows, we describe our model for the ionosphere and the method we have used to estimate the $\boldsymbol{E}$-field available for excitation of UH waves and heating. We then present our results in the form of computed ray trajectories and $\boldsymbol{E}$-field distributions for different cavity placements, before proceeding to a discussion of possible interpretations and implications of our findings. Finally, the most important points are summarised in the conclusions.

2 Notation

Throughout this article, we will use the symbols listed below along with typical values in experiments. Vectors are written in bold italics ($\boldsymbol{A}$, $\boldsymbol{a}$); vector norms and other scalars in italics (A, a). For second rank tensors, we use bold roman (**A**).

c	speed of light in a vacuum
q_e	electron charge
m_e	electron mass
ϵ_0	permittivity of vacuum
n_e	unperturbed ionospheric electron number density
ω_p	plasma frequency; $\omega_\mathrm{p}^2 = \frac{n_\mathrm{e} q_\mathrm{e}^2}{\epsilon_0 m_\mathrm{e}}$
$\boldsymbol{B_0}$	Earth's magnetic field
ω_c	electron gyro (cyclotron) frequency; $\omega_\mathrm{c} = \frac{q_\mathrm{e} B_0}{m_\mathrm{e}}$
$\parallel$, $\perp$	indices denoting vector components parallel/perpendicular to $\boldsymbol{B_0}$
L	scale length of the ionospheric density profile; $L = n_\mathrm{e}/\lvert\nabla n_\mathrm{e}\rvert$
$\boldsymbol{e_b}$	unit vector parallel to $\boldsymbol{B_0}$, with direction chosen such that $\boldsymbol{e_b}\cdot\nabla n_\mathrm{e} > 0$
$\boldsymbol{e_x}$, $\boldsymbol{e_y}$, $\boldsymbol{e_z}$	orthogonal unit vectors forming a right-handed basis, defined by $\boldsymbol{e_z} = \nabla n_\mathrm{e}/\lvert\nabla n_\mathrm{e}\rvert$, $\boldsymbol{e_y} \perp \boldsymbol{B_0}$, and $\boldsymbol{e_x}\cdot\boldsymbol{e_b} \geq 0$
x, y, z	coordinates of a point or indices denoting components parallel to $\boldsymbol{e_x}$ etc.
$\boldsymbol{r}$	spatial position vector; $\boldsymbol{r} = (x, y, z)$
α	angle between $\boldsymbol{e_b}$ and $\boldsymbol{e_z}$; $\cos\alpha = \boldsymbol{e_b}\cdot\boldsymbol{e_z}$. In the unperturbed, horizontally stratified ionosphere, we use $\alpha = 13°$.
l_x	component of $\boldsymbol{e_b}$ perpendicular to $\boldsymbol{e_z}$; $l_x = \sin\alpha$
l_z	component of $\boldsymbol{e_b}$ parallel to $\boldsymbol{e_z}$; $l_z = \cos\alpha$
ω	angular frequency of the pump wave; we use $\omega \approx 3.1\times10^7$ rad/s
$\boldsymbol{k}$	wave vector of the pump wave
θ	angle between $\boldsymbol{e_z}$ and $\boldsymbol{k}$'s projection on the xz plane; $\tan\theta = k_x/k_z$
χ	angle between the wave vector $\boldsymbol{k}$ and $\boldsymbol{B_0}$; $\cos\chi = \boldsymbol{e_b}\cdot\boldsymbol{k}/k$
$\boldsymbol{n}$	refractive index vector; $\boldsymbol{n} = c\boldsymbol{k}/\omega$
X	ω_p^2/ω^2
Y	ω_c/ω; we consistently use $Y \approx 0.26$
$\boldsymbol{E}$	wave electric field
$\boldsymbol{e_E}$	unit vector parallel to $\boldsymbol{E}$; $\boldsymbol{e_E} = \boldsymbol{E}/E$
w	half-width of duct (e.g., $w = 2$ km)
d	maximal relative density depletion in duct (e.g., $d = 3\%$)
W	transmission factor for the Poynting flux

3 Theory

In the theory of cold plasma waves in a magnetized plasma, "L mode" refers to plane waves with wave vector $\boldsymbol{k}$ parallel to $\boldsymbol{B_0}$ and left-handed, circular polarisation with respect to $\boldsymbol{B_0}$ (Swanson, 2003). In terms of the refractive index vector $\boldsymbol{n} = c\boldsymbol{k}/\omega$, L mode waves thus have $n_\perp = 0$. Consequently, in a cold plasma dispersion diagram, the L mode is found along the $\boldsymbol{n} \parallel \boldsymbol{B_0}$ edge of the O and extraordinary (X) mode surfaces (Fig. 1). (Note that this branch of the X mode is sometimes referred to as the Z mode.) Provided the wave angular frequency ω is much larger than the ion plasma and gyro frequencies, the dispersion is given by the Appleton-Hartree dispersion relation:

$$n^2 = 1 - \frac{2X(1-X)}{2(1-X) - Y^2\sin^2\theta \pm \Gamma} \tag{1}$$

where

$$X = \frac{\omega_p^2}{\omega^2} \tag{2}$$

and

$$Y = \frac{\omega_c}{\omega} \tag{3}$$

relate ω to the plasma frequency ω_p and electron gyro frequency ω_c, respectively. Finally,

$$\Gamma = \sqrt{Y^4\sin^4\chi + 4Y^2(1-X)^2\cos^2\chi} \tag{4}$$

also contains the angle χ between the wave vector $\boldsymbol{k}$ and $\boldsymbol{B_0}$.

For $Y < 1$, the dispersion surfaces given by Eq. (1) touch at two radio windows centered at $\omega = \omega_\mathrm{p}$, $n_\perp = 0$, $n_\parallel = \pm\sqrt{Y/(Y+1)}$, one of which is seen in Fig. 1. In a plasma where the density gradient, ∇n_e, is parallel to $\boldsymbol{B_0}$, a pure L mode ($n_\perp = 0$) ray propagating in the direction of increasing plasma density is not affected by the plasma resonance (where $\omega_\mathrm{p} = \omega$) at all – as the ray moves along the z axis, $n_\parallel$ changes continually by refraction and eventually reaches the value $\pm\sqrt{Y/(Y+1)}$, at which point the ray can be said to pass through the radio window, as it moves from the O mode

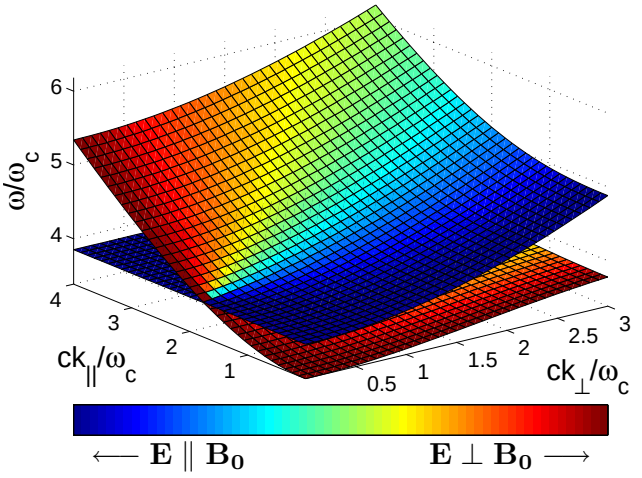

Fig. 1. Dispersion surfaces in the case $\omega_p = 3.85\omega_c$, corresponding to conditions close to the plasma resonance (where $\omega_p = \omega$) for $Y \approx 0.26$. The L mode is represented by the left-hand edge ($n_\perp = 0$) of the O mode (for $\omega_p > \omega$) and X (or Z) mode (for $\omega_p < \omega$) surfaces. Note that $\boldsymbol{E} \perp \boldsymbol{B_0}$ on this edge (red = perpendicular polarisation; blue = parallel polarisation). These surfaces are deformed as the ray moves through the ionosphere, so that the point defined by ω and $\boldsymbol{k}$ of the ray always lies on one of the surfaces. Cf. Swanson, p. 53f.

to the X mode surface in Fig. 1. It keeps propagating on the other side until encountering the L mode cutoff at

$$\omega_L = -\frac{\omega_c}{2} + \frac{1}{2}\sqrt{\omega_c^2 + 4\omega_p^2}. \tag{5}$$

To understand what happens when $n_\perp$ is nonzero, we note that as the ray propagates through the ionosphere, refraction causes its refractive index $\boldsymbol{n}$ to trace a curve in $\boldsymbol{n}$-space. If this curve passes close enough to one of the points $n_\perp = 0$, $n_\parallel = \pm\sqrt{Y/(Y+1)}$, i.e., the radio windows, some transmission will occur. Since $n_\perp$ is unaffected by refraction when $\nabla n_e \parallel \boldsymbol{B_0}$, while $n_\parallel$ still attains $\pm\sqrt{Y/(Y+1)}$ at some point along the trajectory, the minimum $\boldsymbol{n}$-space distance to the window is $\sigma_{min} = n_\perp$. Of the incoming energy, only a factor W now gets through, where

$$W = \exp\left(\frac{\pi\omega L}{2c}\sqrt{\frac{Y}{Y+1}}\sigma_{min}^2\right) \tag{6}$$

with $L = n_e/|\nabla n_e|$ denoting the scale length of ionospheric density variation (Mjølhus, 1990). Equation (6) is valid for

$$Y\left(\frac{\omega L}{c}\right)^{2/3} \gg 1 \tag{7}$$

where the LHS gives the number of Airy wavelengths between the plasma resonance and the L mode cutoff.

From Eq. (6), we can interpret

$$\xi = \left(\frac{\pi\omega L}{2c}\sqrt{\frac{Y}{Y+1}}\right)^{-1/2} \tag{8}$$

as the width of each radio window in refractive index space.

In the ionosphere, ∇n_e and $\boldsymbol{B_0}$ are of course usually not parallel. However, the reasoning is easily generalised to cover this situation as well. To this end, we use the coordinates described in Sect. 2, which have ∇n_e aligned with the z axis and the y axis perpendicular to $\boldsymbol{B_0}$ and ∇n_e. In these coordinates, the radio window at $n_\perp = 0$, $n_\parallel = \pm\sqrt{Y/(Y+1)}$ is given by

$$n_x = \pm l_x\sqrt{Y/(1+Y)} \equiv \sin\theta_{crit} \equiv n_{crit} \tag{9}$$

$$n_y = 0 \tag{10}$$

$$n_z = \pm l_z\sqrt{Y/(1+Y)}. \tag{11}$$

Here, we defined the critical angle of incidence, θ_{crit}, and the critical index of refraction, n_{crit}, and let l_x and l_z denote $\sin\alpha$ and $\cos\alpha$, respectively, where α is the angle between $\boldsymbol{B_0}$ and ∇n_e. Under the conditions considered in this paper ($Y \approx 0.26$ and $\alpha = 13°$, typical for experiments at the European Incoherent Scatter scientific association (EISCAT) facility near Tromsø, Norway), Eq. (9) gives $\theta_{crit} \approx \pm 6°$.

Since $\nabla n_e \parallel \boldsymbol{e_z}$, n_x and n_y now remain unchanged by refraction, while n_z changes. The minimum $\boldsymbol{n}$-space distance to the window thus becomes

$$\sigma_{min} = \sqrt{(n_x - n_{crit})^2 + n_y^2}, \tag{12}$$

which reduces to $n_\perp$ for $\alpha \to 0$. The transmission factor W is obtained by inserting Eq. (12) into Eq. (6).

Some rays reaching the neighbourhood of one of the radio windows in a plane stratified ionosphere are plotted in Fig. 2. The ray in the centre was launched with $k_x/k_z = \tan\theta_{crit}$. As a consequence, it propagates in the L mode at the plasma resonance and is fully transmitted. Note also the polarisation, which for this ray stays perpendicular all the way up to the L mode reflection altitude, while the surrounding O mode rays acquire increasingly parallel polarisation as they approach the plasma resonance.

If the ionosphere is plane stratified, n_x and n_y are given by the corresponding directional cosines of $\boldsymbol{k}$ before the wave enters the ionosphere. However, we choose to use the refractive index to emphasize that the same formulas hold in an ionosphere which is only locally plane stratified, such that the direction of $\boldsymbol{e_z}$ slowly changes as the wave propagates and n_x and n_y are not equal to their values at incidence.

4 Model and computational method

The ionosphere we have used has a Chapman plasma density profile, $n_{e0}(z)$, modified by a long, cylindrical, magnetic field aligned region of lower density. The total plasma density is thus given by $n_e(\boldsymbol{r}) = n_{e0}(z) + dn_e(\boldsymbol{r})$, where $dn_e(\boldsymbol{r})$ represents the density reduction. Noting the wave guiding properties of the density perturbation, we will refer to it as an ionospheric duct. Our attention is confined to ducts located in the meridional (xz) plane.

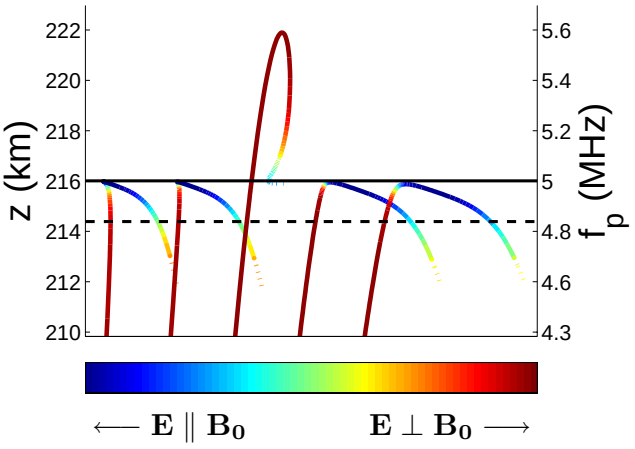

Fig. 2. Ray paths in a plane stratified Chapman ionosphere with scale length $L_0 = 40$ km and a maximum electron density of $n_{\max} = 8 \times 10^{11}\,\mathrm{m}^{-3}$ at $h_0 = 275$ km. Radio window rays are converted into the X (or Z) mode at the plasma resonance ($\omega = \omega_\mathrm{p}$), then propagate to even higher altitudes. Note that rays with inclination angle $\theta < \theta_c$ also reach $\omega_\mathrm{p} = \omega$, but reflect in a Spitze. The colour coding shows the polarisation of the rays. The solid black line marks the location of the plasma resonance, while the dashed line corresponds to the UH resonance.

The Chapman background has a maximum electron density of $n_{\max} = 8 \times 10^{11}\,\mathrm{m}^{-3}$ at height $h_0 = 275$ km and scale length $L_0 = 40$ km. For the duct, $\delta_\mathrm{e}(\boldsymbol{r})$, we use a gaussian function with a half-width w of a few kilometres and a maximal density reduction d on the order of a few percent:

$$\delta_\mathrm{e}(\boldsymbol{r}) = -d \exp\left[-\frac{(x - x_\mathrm{duct}(z))^2 + y^2}{w^2}\right] \tag{13}$$

where

$$x_\mathrm{duct}(z) = x_\mathrm{duct}(0) + z\tan\alpha \tag{14}$$

is the x coordinate at the centre of the duct. By varying $x_\mathrm{duct}(0)$, we shift the position of the duct along the x-axis – for instance, $x_\mathrm{duct}(0) = 0$ corresponds to a duct in the MZ.

For the most part, the prescribed plasma density varies slowly compared to the wavelength of high frequency radio waves. Therefore, we can use ray tracing to describe the propagation of the waves. The slow variation also permits us to neglect partial reflection (Budden, 1985, p. 166). Nor do we include the effects of absorption. The ray tracing consists in integrating a set of Hamilton's equations corresponding to Eq. (1). We use Matlab's ode45, a Runge-Kutta type ordinary differential equation solver, to perform the computation.

After tracing the rays, we turn to determining $\boldsymbol{E}$ along each ray. Using Faraday's law and the definition of the cold plasma dielectric tensor $\boldsymbol{\epsilon}$, which in a coordinate system where the z axis is aligned with $\boldsymbol{B_0}$ becomes (Swanson, 2003, p.24)

$$\boldsymbol{\epsilon} = \begin{pmatrix} S & -iD & 0 \\ iD & S & 0 \\ 0 & 0 & P \end{pmatrix}, \tag{15}$$

where (neglecting ion motion)

$$S = 1 - \frac{\omega_\mathrm{p}^2}{\omega^2 - \omega_\mathrm{c}^2} = 1 - \frac{X}{1 - Y^2} \tag{16}$$

$$D = \frac{\omega_\mathrm{c}\omega_\mathrm{p}^2}{\omega(\omega^2 - \omega_\mathrm{c}^2)} = \frac{XY}{1 - Y^2} \tag{17}$$

$$P = 1 - \frac{\omega_\mathrm{p}^2}{\omega^2} = 1 - X \quad , \tag{18}$$

we obtain

$$\boldsymbol{k} \times (\boldsymbol{k} \times \boldsymbol{E}) + \frac{\omega^2}{c^2}\,(\boldsymbol{\epsilon}\ \boldsymbol{E}) \equiv \mathbf{A}(\boldsymbol{k})\ \boldsymbol{E} = 0. \tag{19}$$

Since we are only interested in the nontrivial solution of this equation, we require the determinant of the coefficient matrix $\mathbf{A}(\boldsymbol{k})$ to be zero. After some reformulation, this leads to Eq. (1). Selecting one or the other of the roots, depending on which mode we are investigating, we find the direction $\boldsymbol{e_E}$ of $\boldsymbol{E}$ for any given $\boldsymbol{k}$ by calculating the nullvector of Eq. (19) associated with that root.

In order to determine also the amplitude of $\boldsymbol{E}$, we consider the Poynting flux,

$$\langle \boldsymbol{S} \rangle = \frac{1}{2}\,\Re(\boldsymbol{E} \times \boldsymbol{H}^*), \tag{20}$$

where

$$\boldsymbol{H} = \frac{1}{\epsilon_0 n}\,\boldsymbol{k} \times \boldsymbol{D}\ , \tag{21}$$

$$\boldsymbol{D} = \boldsymbol{\epsilon}\ \boldsymbol{E}, \tag{22}$$

while $\Re$ stands for taking the real part and *denotes complex conjugation. Using $\boldsymbol{E} = E\boldsymbol{e_E}$, this can be written in the form

$$\langle \boldsymbol{S} \rangle = |E|^2\ \boldsymbol{a}(\boldsymbol{e_E}). \tag{23}$$

We use Eq. (23) together with Eq. (19) and an independent estimate for $\langle \boldsymbol{S} \rangle$ to solve for the field amplitude E. The estimated Poynting flux, $\langle \boldsymbol{S} \rangle_\mathrm{est}$, is obtained by grouping neighbouring rays into bundles and keeping track of the cross-sectional area between them, then applying conservation of energy, taking into account the power output from the transmitter. To find the best fit between $\langle \boldsymbol{S} \rangle_\mathrm{est}$ and $\langle \boldsymbol{S} \rangle$ in the least squares sense, we require that ($a = |\boldsymbol{a}|$)

$$\frac{1}{a^2}\,(\langle \boldsymbol{S} \rangle_\mathrm{est} \cdot \boldsymbol{a})\boldsymbol{a} = |E|^2 \boldsymbol{a} = \langle \boldsymbol{S} \rangle\ . \tag{24}$$

Consequently,

$$|E| = \sqrt{\frac{1}{a^2}\,\langle \boldsymbol{S}_\mathrm{est} \rangle \cdot \boldsymbol{a}}\ . \tag{25}$$

Naturally, the argument does not provide any information about the phase φ of $\boldsymbol{E}$, which could on the other hand be obtained by integrating the wave vector along the ray.

The procedure described above yields a succession of plane waves with field direction and amplitude determined by local plasma properties. This can be regarded as the Wentzel-Kramers-Brillouin (WKB) solution to the problem. Accordingly, this solution is only valid where the usual WKB requirements are met. For instance, the wavelength has to be small compared to the density scale length, which is true only sufficiently far from the plasma resonance – close to the resonance, a full wave solution would be necessary. (Alternatively, complex raytracing might be useful; cf. Budden (1980).) Budden (1985, p. 489) gives a condition for the applicability of WKB in terms of the parameter $q = n\cos\chi$, which contains the refractive index, $n = ck/\omega$, and the angle χ between $\boldsymbol{k}$ and $\boldsymbol{B_0}$. The q given by raytracing always equals one root of the Booker quartic equation. According to this criterion, WKB holds when

$$\frac{c}{\omega}\left|\frac{\mathrm{d}}{\mathrm{d}z}\left(\frac{1}{q-q_j}\right)\right| \leq 1\,, \tag{26}$$

where q_j, $j = (2,3,4)$ represents the remaining three roots of the Booker equation.

We use Eq. (26) to see when to interrupt the ray tracing. At this point, we compute the transmission (conversion) coeffient given by Eq. (6). If the transmission exceeds a certain threshold, we make a leap in the direction of ∇n_e and continue the integration from a point 50 m above the resonance, adjusting the wave number parallel to ∇n_e (i.e., k_z) to satisfy the dispersion relation, but keeping the other components of $\boldsymbol{k}$ unchanged. A similar method was used by Papagiannis and Miller (1969). Poynting flux computed above the plasma resonance is reduced by W.

Since the length of the jump across the plasma resonance is arbitrarily chosen, our treatment of the transmission introduces some errors that might be avoided in a more sophisticated approach. For instance, rays which are not transmitted through the very centre of the radio window are inclined towards the horizontal just after transmission, which means that an error in the vertical direction is translated into a horizontal displacement of the ray after transmission. This in turn affects the calculation of the Poynting flux, though only locally. The total transmitted Poynting flux is still conserved in this case.

Another kind of error arises from occasional computational difficulty of choosing the right root of the dispersion equation after transmission. In the relatively few cases where this problem occurs (notably in connection with ducts between the vertical and the customary location of the radio window), the integration is interrupted. In future versions of the code, this could be remedied by checking that the new value of q is indeed on the right branch of the Booker quartic equation. In contrast to the case of mere ray displacements, the premature interruption of rays leads to a reduction in the total Poynting flux. However, since rays passing close to the centre of the radio window are generally not subject to the effect, the regions of most intense transmission are not affected.

WKB also breaks down in the vicinity of caustics, where the amplitude of $\boldsymbol{E}$ goes to infinity. A criterion for when a full wave treatment is necessary in this case was derived by Budden (1961). However, since fine structure is not the main focus of the present study, we use ray tracing throughout, but reduce spurious small scale effects by only considering 200-by-200 m squares in the horizontal plane. This also minimises errors stemming from ray displacements due to the jump across the plasma resonance.

For each 200-by-200 m square, we compute the average $\boldsymbol{E}$ by summing the contributions to the field from all ray bundles intersecting the square, neglecting the phase difference between overlapping bundles. Taking relative phase shifts into account would introduce interference patterns, but would not significantly change the overall picture.

As mentioned above, we use the cross-sectional area of the ray bundles to estimate the Poynting flux. Other methods also exist; for instance, an equation for the ray separation distance can be included in the integration. For each individual ray, this would give a more exact result (Budden, 1985, p. 414). On the other hand, the approach we have used here is simpler and faster, while still providing sufficient accuracy for our needs. Also, any overlapping of rays from different parts of the beam due to focussing is automatically taken care of when we sum the contributions to $\boldsymbol{E}$ from all ray bundles. Even if we used a method based on individual ray paths, this type of summation would be necessary in order to obtain the total field.

5 Results

We have performed ray tracings for a selection of duct widths, depths and locations. Some general trends and features of the results will now be summarised, with special focus on the transmission through the plasma resonance. Since transmission occurs when rays are propagating in the L mode (see Sect. 3), which is characterised by perpendicular polarisation, all results regarding transmission give information about the efficiency of UH excitation in small scale striations – also for altitudes below the plasma resonance. (Of course, UH oscillations can only be excited provided the plasma density is such that $\omega_\mathrm{UH} < \omega$ holds inside the striations while at the same time $\omega_\mathrm{UH} > \omega$ in the ambient plasma, where $\omega_\mathrm{UH} = \sqrt{\omega_\mathrm{p}^2 + \omega_\mathrm{c}^2}$ is the UH frequency. However, a mere 10% density depletion on the small scale is sufficient for this condition to be fulfilled in an altitude range stretching from the background UH resonance up to several kilometres above the plasma resonance.)

The transmission factor is determined by quantities that are affected by plasma density gradients (e.g., the angle

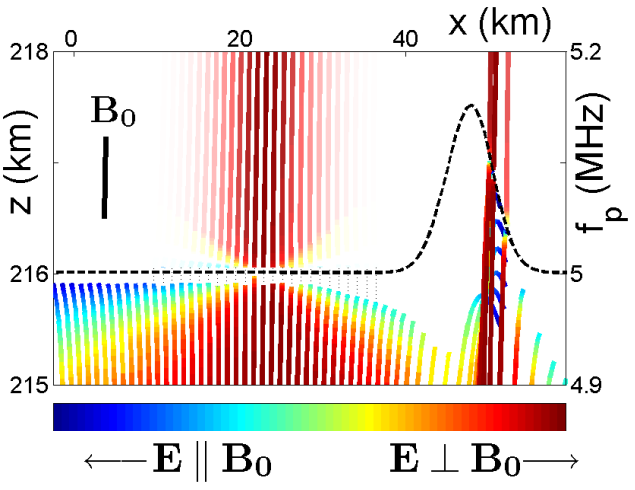

Fig. 3. Ray paths in the meridional (xz) plane in a Chapman ionosphere modified by a cylindrical duct close to the MZ. The transmitter is at $x = z = 0$. The duct has width $w = 4$ km and depth $d = 6\%$, and allows rays directed towards the MZ to pass through the radio window. The orientation of $\boldsymbol{B_0}$ is indicated by a black line on the left. As in Fig. 2, the polarisation of the rays is colour-coded, while the increased brightness of lines away from the centre of the radio window reflects the loss of power during the course of transmission through the plasma resonance. The dashed black line marks the location of the plasma resonance ($f_p = 5$). The raytracing is interrupted when WKB is no longer valid, or when the ray turns and starts propagating towards decreasing plasma density.

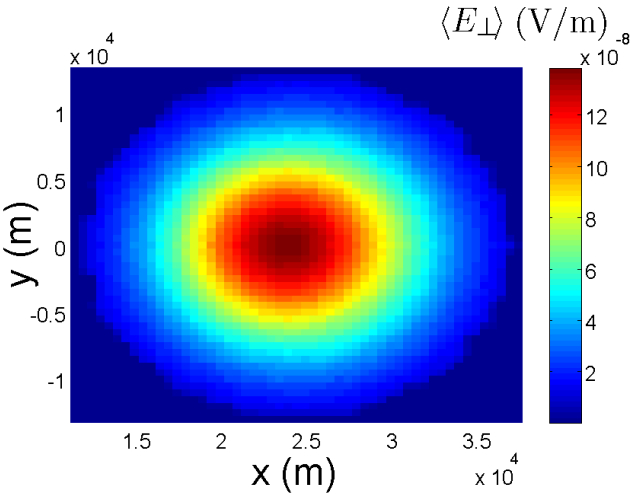

Fig. 4. Cross section of the transmitted part of the beam at $X \approx 1.2$, i.e., a few kilometres above the plasma resonance, around the radio window at $\theta \approx 6°$, in a horizontally stratified ionosphere. The coloured patches represent 500-by-500 m squares, the colour corresponding to $\langle E_\perp \rangle$, the average value of $E_\perp$ inside each square, where $E_\perp$ is the wave electric field component (in V/m) perpendicular to the magnetic field. The field was computed assuming a 10° beam of 3.6 MW total power, roughly corresponding to the HAARP transmitter. This gives a maximum electric field $\langle E_\perp \rangle_{\max}$ of around 1.3×10^{-7} V/m. However, since absorption has not been included, a real-world experiment would yield much weaker fields.

between the density gradient and the magnetic field). These gradients also give rise to focussing effects that influence the shape of the radio beam. Thus, it is not surprising that ducts corresponding to similar gradients exhibit similar transmission patterns. For instance, the transmission in a $w = 4$ km, $d = 6\%$ duct resembles the case of a $w = 2$ km, $d = 3\%$ duct at a slightly shifted location (differences between the cases will be pointed out below).

Figure 3, which shows ray paths between the vertical and the MZ in the presence of a $w = 4$ km, $d = 6\%$ duct, therefore gives a fairly representative picture of the results. In addition to the broad transmission through the ordinary radio window, a set of rays guided by the duct are seen to cross the plasma resonance. Figures 4 and 5 show cross sections in the xy plane of the transmitted parts of the beam.

If we keep the width and depth of the duct fixed while varying its location, we see that the transmission changes in a rather straightforward way. Close to the original critical angle, the effect of the cavity is seen as a perturbation of the broad transmission through the radio window of a plane stratified ionosphere. In this region, a cavity cannot be expected to increase the overall transmission, only redistribute it. However, this redistribution can yield quite dramatic results, as seen in Fig. 6, where a depletion is made to coincide with the radio window. While the transmission through the

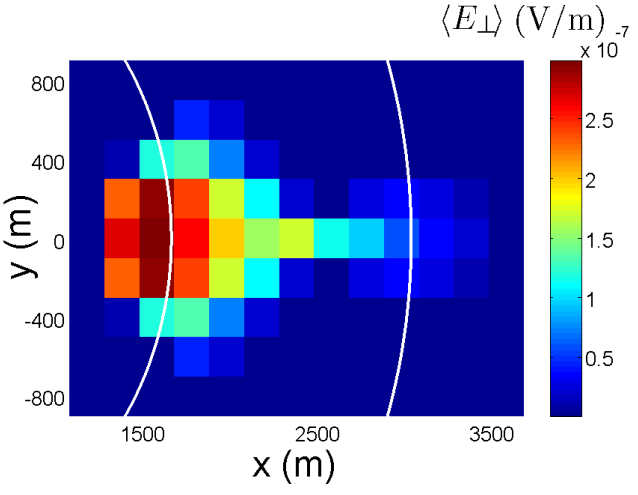

Fig. 5. Cross section at $X \approx 1.2$ in a duct with $w = 2$ km and $d = 3\%$. The coordinate system has here been centered at the duct. White arcs mark the 1.5% (left arc) and 0.3% (right arc) density depletion levels. The perpendicular electric field, this time averaged over 200-by-200 m squares, now reaches a maximal value of $\langle E_\perp \rangle_{\max} \approx 3 \times 10^{-7}$ V/m. Other duct placements give different values of the maximal field; see Fig. 7.

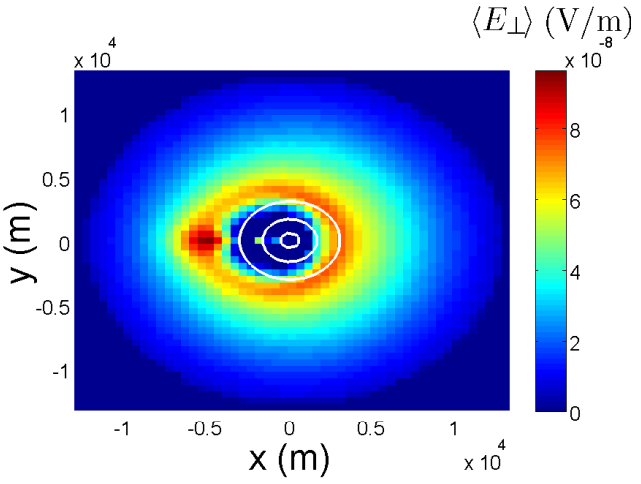

Fig. 6. The transmitted part of a beam directed at the radio window at $\theta \approx \pm 6°$, when the ionosphere has a $w = 2$ km, $d = 3\%$ duct. Again, the cross section is made at $X \approx 1.2$, and the coordinate system is centered at the duct. The white circles mark the 10%, 50% and 90% levels of relative density depletion, respectively. In other words, the outer circle shows where the depletion is 0.3%, the middle one where it is 1.5%, and the inner circle tells us where the density is 2.7% below the unperturbed value.

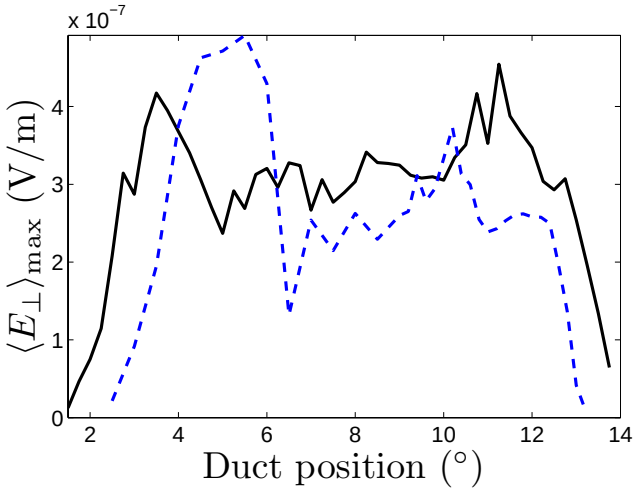

Fig. 7. The black, solid line shows the maximal averaged wave perpendicular electric field above a duct similar to the one of Fig. 5 ($w = 2$ km, $d = 3\%$), for different duct locations in the meridional plane. The position of the duct is indicated by the angle between the vertical and a straight line connecting the site of emission with the point where the centre of the duct passes through the plasma resonance. For instance, if $\alpha = 13°$, a duct at 13° is perceived to lie in the magnetic zenith. The blue, dashed line corresponds to a $w = 1$ km, $d = 1.5\%$ duct.

centre of the window is almost entirely wiped out, we note a strong, narrow peak just outside the cavity. This shifted, concentrated radio window transmission becomes even more pronounced when the cavity is moved a few degrees towards the vertical (cf. Fig. 7).

As we move the cavity in the opposite direction, i.e., towards the MZ, the distinct transmission pattern of Fig. 5 emerges. While the total transmitted power falls off as we move away from the radio window, the peak transmitted power reaches a maximum when the cavity is a few degrees from the MZ (Fig. 7). In other words, the broad transmission of the unperturbed radio window is succeeded by one or several patches of more concentrated transmission.

It is clear from Fig. 7 that the results do vary somewhat if we for instance change the dimensions of the duct (this will be further discussed in Sect. 6). The picture would also change to some extent if we looked at another altitude. Furthermore, the maximal electric field depends strongly on the scale over which we average (indeed, the field would go to infinity if we closed in on a caustic). This also influences the relative height of the peaks, since the degree of focussing is not the same for all duct positions. With all this said, the graph does give an idea of the combined effect of transmission and focussing as the duct is translated in the meridional plane.

6 Discussion

To understand the results, we have to look at the relation between refraction and transmission. The most crucial effects of refraction are (1) to focus the rays and thereby create high intensity patches, (2) to influence the polarisation of the rays, and (3) to determine which rays are transmitted through the plasma resonance. In other words, density perturbations do not only act as lenses, but can also help waves maintain perpendicular polarisation, as well as shift the position of the radio window or introduce radio windows at entirely new locations. When these effects combine, strong perpendicular fields appear above the plasma resonance.

For instance, the strong peak for a $w = 1$ km, $d = 1.5\%$ duct at 5.5° in Fig. 7 is a result of favourable conditions for transmission occurring in a region where the duct is able to focus rays efficiently. For a duct which is twice as wide and deep, a qualitatively similar enhancement is seen at 3.5°, but the peak is slightly lower in this case, partly because focussing becomes less pronounced as we approach the vertical. This in turn can be interpreted as a result of the fact that rays propagating at a small angle to the axis of a duct are subjected to refraction over a longer distance. Since the ducts are field aligned, having them located vertically above the transmitter implies a large angle of incidence for incoming rays and consequently weaker focussing. Conversely, ducts close to the MZ act as wave guides – i.e., rays are captured and forced to propagate along the duct (cf. Fig. 10).

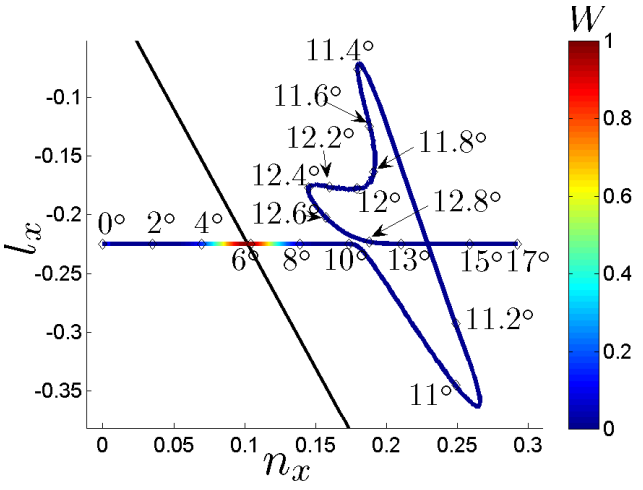

Fig. 8. The parameters of Eq. (9), n_x and l_x, plotted for a succession of rays in the meridional plane. The values of n_x and l_x are taken at the point of closest approach to the plasma resonance. The ionosphere has a $w = 2$ km, $d = 1.5\%$ density reduction close to the magnetic zenith. The black line represents the radio window at $n_x = -l_x\sqrt{Y/(1+Y)}$. The colour indicates the transmission factor, which reaches 1 at the radio window, $\theta = \theta_{\rm crit} \approx \pm 6°$ (cf. Fig. 3).

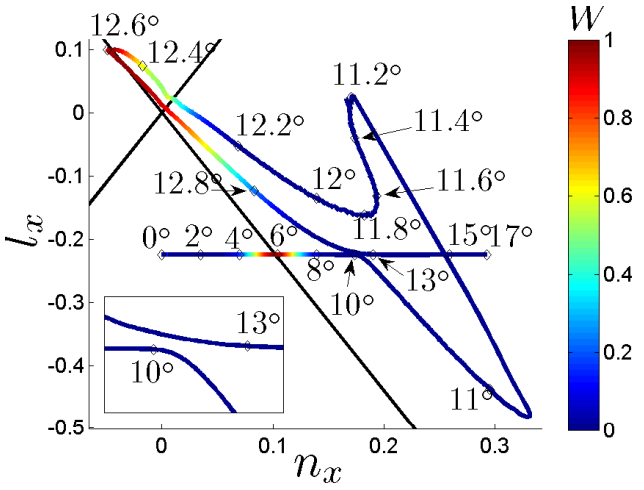

Fig. 9. Similar to Fig. 8, but for a $w = 2$ km, $d = 3\%$ duct. The curve now returns to the $n_x = -l_x\sqrt{Y/(1+Y)}$ line, as rays propagating in the duct reach the radio window and are transmitted (the two points where the curve crosses the line correspond to two fully transmitted rays). Note that this additional radio window appears where $\boldsymbol{B_0}$, $\nabla n_{\rm e}$ and $\boldsymbol{k}$ are close to parallel. The second window, at $n_x = +l_x\sqrt{Y/(1+Y)}$, is seen as another line, crossing the first one at right angles in the upper left corner of the figure. Transmission through this window, however, does not lead to propagation above the plasma resonance and has therefore not been considered in this study.

For a discussion of duct-related focussing phenomena in the VLF case, see the article by Starks (2002).

We next consider the transmission factor, which is obviously affected by the introduction of ducts. To some extent, the 'new' radio windows can be explained by the tilting of the density gradient ($\nabla n_{\rm e}$) in the duct, which alters the critical angle for transmission. On the northern or upper side of the duct, where $\nabla n_{\rm e}$ is tilted away from $\boldsymbol{B_0}$, the window is shifted towards the vertical, while on the southern or lower side of the duct, the window moves towards larger inclinations. Consequently, some rays that normally would not reach the radio window should be able do so when passing through a duct. North of the ordinary critical angle, where incoming rays would normally be too close to the vertical to be transmitted, transmission would thus become more likely for rays passing through a region where the northern side of a duct intersects the plasma resonance, in agreement with the transmission peak north of the duct in Fig. 6. Conversely, transmission would primarily occur on the southern side of a duct located south of the critical angle (cf. Fig. 5).

However, we also have to consider the effect of refraction in the duct on the propagating radio waves. We have already mentioned focussing, but equally important from our point of view is the fact that refraction tilts the wave normal, which has implications for the transmission factor. For instance, rays propagating along the northern side of a duct have their wave normals pushed away from the vertical; simultaneously, the radio window moves towards the vertical, by the argument above. Taking refraction into account, the transmission patterns expected from changes in the critical angle should thus be even more pronounced.

The effects described above are clearly discernible in Figs. 8, 9 and 11, where we plot the parameters $n_x = \sin\theta$ and $l_x = \sin\alpha$ for a set of rays in the meridional plane (i.e., rays with $n_y = 0$ and different initial values of n_x), with the values of n_x and l_x taken at the point of closest approach to the plasma resonance before transmission. Recall Eq. (9), which gives the location of the radio windows in terms of n_x and l_x. The radio window we are interested in is reached by rays with $n_x = -l_x\sqrt{Y/(1+Y)}$.

In a plane stratified ionosphere, l_x is a constant, and n_x is constant along each individual ray. Accordingly, our set of rays would correspond to a straight, horizontal line in the n_x and l_x plane. When a duct is introduced, however, the line is gradually bent as l_x and n_x both deviate from their unperturbed values, as we can see in Fig. 8.

At $w = 2$ km, $d = 1.5\%$, the duct of Fig. 8 is not deep enough to introduce additional radio windows close to the MZ. When we increase the maximal depth to 3%, however, the n_x and l_x curve traced by a set of rays in the meridional plane becomes sufficiently distorted by the duct to cross the line $n_x = -l_x\sqrt{Y/(1+Y)}$ (Fig. 9). The rays represented by this part of the curve are partly or completely transmitted (Fig. 10).

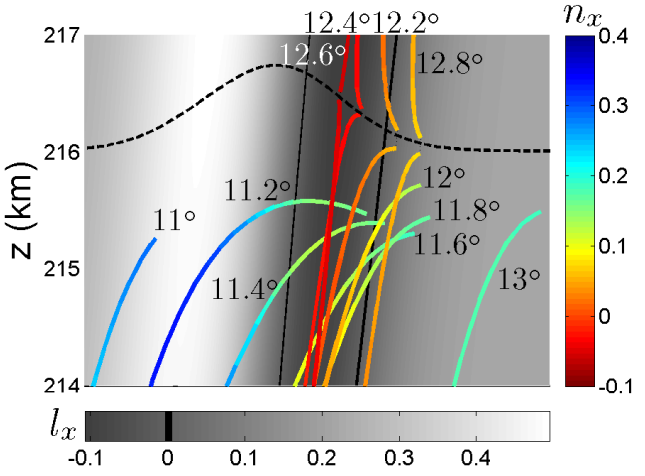

Fig. 10. Some of the rays included in Fig. 9. The gradual shift in the value of l_x, which is given by the angle between the magnetic field and the density gradient, is here illustrated by the grayscale background shading, while n_x, which depends on the direction of the wave vector along each ray, is indicated by the ray colour. The continuous black curve shows where $\boldsymbol{B_0}$ and ∇n_e are antiparallel ($l_x = 0$), while the dashed black curve marks the location of the plasma resonance. To keep the figure from becoming too cluttered, the x axis, corresponding to the horizontal coordinate, has been omitted (cf. Fig. 3).

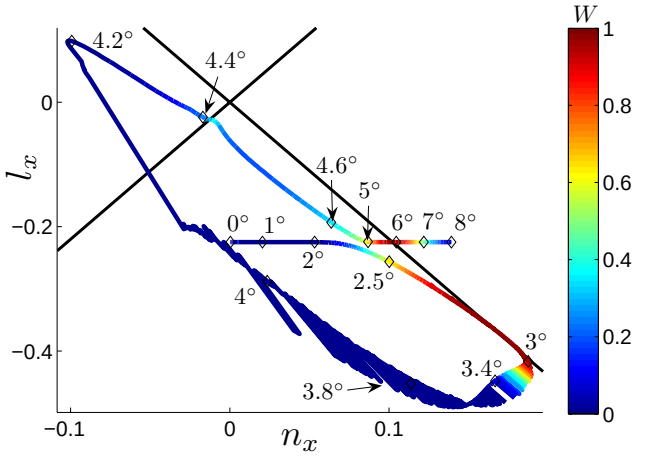

Fig. 11. When the $w = 2$ km, $d = 3\%$ density duct is placed north of the usual location of the radio window, at 3.5° from the vertical, the n_x vs. l_x diagram for a set of meridional rays reveals a radio window at an entirely different location compared to Fig. 9 (cf. Fig. 12).

Another way to look at the transmission is to note that a deep enough field aligned density cavity contains a region in space where ∇n_e is approximately parallel to $\boldsymbol{B_0}$. A ray that enters this region with a sufficiently small angle of incidence continues to propagate along $\boldsymbol{B_0}$, and is efficiently transmitted. This ray neatly fits the textbook description of the L

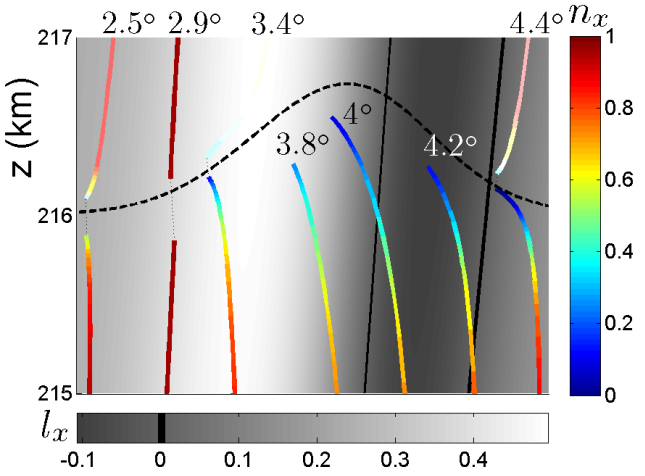

Fig. 12. Ray paths in the vicinity of a $w = 2$ km, $d = 3\%$ duct at 3.5°, corresponding to Fig. 11. Transmission now mainly takes place on the northern side of the duct, as expected from Fig. 6, although the relative proximity to the original radio window also allows rays south of the duct to be transmitted (e.g. the ray at 4.4°). Only select rays are plotted here. Some of the rays between 2.9° and 3.4° were interrupted due to the numerical problem discussed in Sect. 4.

mode. From this point of view, then, achieving strong transmission is a matter of having a large number of rays entering straight into the region of field aligned density gradients. We see from Figs. 9 and 10, where $\boldsymbol{B_0}$, ∇n_e and $\boldsymbol{k}$ are indeed close to parallel in the region of strong transmission, that this interpretation makes sense for ducts south of the customary radio window location – though not for ducts close to the vertical (cf. Fig. 12).

Figure 7 suggests that ducts relatively close to the MZ (duct position $\sim 11.5°$ for a $w = 2$ km, $d = 3\%$ duct; $\sim 10.2°$ for a $w = 1$ km, $d = 1.5\%$ one) give rise to particularly strong perpendicular electric fields, which would imply a preference for UH wave excitation in that direction. On the other hand, the peak at $\sim 3.5°$ or $\sim 5.5°$ has similar or even larger amplitude, which means that we cannot explain the MZ effect by looking at the maximal fields only. Also, it is important to remember that while the maximal field may reach its peak value in a duct at 11.5°, the radio window of a plane stratified ionosphere generally gives higher total transmitted power.

From a self-focussing point of view, however, one important circumstance does speak in favour of the ducts close to the MZ: the fact that in these cases, the region of strong fields is found close to the centre of the duct (cf. Fig. 5). This obviously has to do with guiding of the rays, which, as we noted above, is more likely to occur in ducts close to the MZ. Consequently, the induced heating is to a higher extent contained inside the duct, which could be vital to maintaining or even enhancing the density depletion.

It is interesting to compare our results with the empirical model by Pedersen et al. (2008) for HF radio-induced optical emission production efficiency. In a beam-swinging experiment conducted at the High Frequency Active Auroral Research Program (HAARP) facility in Alaska, USA, it was found that optical emissions are most effectively produced in a $\sim 15^\circ$ wide region, slightly elongated in the north-south direction and centered at a point between the vertical and the MZ, with a superimposed, $\sim 7^\circ$ wide gaussian peak in the MZ. The study includes ray tracings in a time-dependent ionosphere without field aligned density perturbations. Since these tracings do not single out the region of strongest emissions, the authors conclude that the production efficiency pattern is most likely not due to propagation conditions.

In order to test this interpretation, a natural step would be to study propagation through a distribution of irregularites, and in particular to look at the combined effect of several ducts. While the results presented here are valid in the case of well separated ducts, in the sense that the density depletions do not overlap and also that rays do not traverse several depletions before reaching the interaction region, closely spaced ducts would call for a new round of ray tracings. Unless a specific model for the distribution of ducts is proposed, one would then have to examine a large number of possible configurations. Although interesting, this type of extensive investigation falls outside the scope of the present study.

However, given our findings (cf. Fig. 7), it seems probable that the inclusion of several kilometre-scale ducts in the model ionosphere would yield a plateau stretching between the vertical and the MZ, similar to the one observed by Pedersen et al. (2008) – that is, if the optical emissions are assumed to correlate with the maximal perpendicular wave electric field strength at altitudes above the plasma resonance. One reason to expect high altitude fields to play an important role is the fact that the zeroth order (and hence uppermost) resonance for UH generation inside a striation gives the largest contribution, as explained by Mjølhus (1998). But we have also seen how ducts help the wave field stay perpendicularly polarised, which in turn facilitates the excitation of UH waves (Leyser and Nordblad, 2009). On top of this, focussing effects are in play, producing regions of intense fields e.g. at the UH resonance, which otherwise might not be reached at all. In other words, situations which exhibit strong transmitted fields can also be assumed to produce stronger effects at lower altitudes, further underlining the importance of ducted propagation. Incidentally, this also means that ducts could be relevant even in cases where the frequency of the pump exceeds the maximal plasma frequency, or when absorption is too strong for the rays to reach the plasma resonance.

We hope that future experiments will provide opportunities to confirm the conclusions of our work. In particular, valuable information could be obtained from observations of optical emissions in the confirmed presence of ducts created by natural processes or artificially by pumping. Simultaneous rocket density measurements like those performed by Kelley et al. (1995) would be extremely useful in this regard. A duct at the location of the radio window should for instance give rise to annular emissions, according to Fig. 6, which could be easily verified as soon as the density profile is known with sufficient precision.

There are also indirect ways to observe duct-related phenomena. The so-called Z mode trace, sometimes seen in ionograms (Ellis, 1956), is one sign of transmission. If the peak ionospheric plasma density, which can be measured using an ionosonde, is so low that the L mode cutoff is never encountered (cf. Eq. 5), we can also expect reflection of the pump wave from the topside plasma resonance, as well as tunneling of part of the transmitted power into space. Observations by passing satellites during such conditions would thus offer a powerful test of our model.

One interesting study of topside effects was conducted by Isham et al. (1999), who observed heater-induced topside enhancements of the ion and plasma lines using the UHF and VHF incoherent scatter radars at EISCAT. As the UHF radar scanned between vertical and geomagnetic field-aligned, it became clear that topside enhancements occurred principally between the radio window and geomagnetic field-aligned position. The authors noted that these results are incompatible with a single, narrow radio window. On the other hand, the occurrence of topside excitations at a wide range of angles away from the radio window is consistent with the model of L mode propagation presented in this paper. However, the pump duty cycle used in the experiments (0.2 s on/9.8 s off) was probably too low for the pump to induce large scale density irregularities that could guide the pump into the L mode. Furthermore, Isham et al. pointed out that considering the smoothness of the high range resolution data, it seemed unlikely that the ionosphere was perturbed by density irregularities. Nonetheless, we suggest that natural kilometer-scale density ducts may have been present during the experiment. Such depletions would have to be deep enough to produce transmission of the pump wave, but not so deep as to shift the location of the plasma resonance by more than a few hundred metres, given the smoothness of the data. But this is clearly possible, as can be concluded from Fig. 10, where a relatively deep duct (width $w = 2$ km, depth $d = 3\%$), eminently capable of producing transmission, is seen to lift the plasma resonance by less than a kilometre.

In addition, it is interesting to note that Isham et al. inferred an atmospheric wave propagating through the pump–ionosphere interaction region. Such a wave could have tilted the ionospheric density gradient parallel to the geomagnetic field, which would also facilitate L mode propagation of the pump wave. Similarly, Bowman (1960) observed Z mode traces in ionograms obtained from an ionosphere tilted by spread-F irregularities.

Mishin et al. (2001) interpreted the topside enhancements in terms of resonant scatter on small scale field-aligned striations, where the O-mode pump wave scatters into Z waves

that can propagate to the topside ionosphere. To discriminate between this scattering process and our model of L mode propagation one can study the temporal evolution. In a plane stratified ionosphere, without pre-existing large scale ducts, the resonant scattering into Z waves should occur already after a few seconds, as determined by the time scale for the evolution of small scale striations. On the other hand, the formation of the large scale ducts that are needed for L-mode guiding takes on the order of a minute. This long evolution time is consistent with that for the self focusing observed by Kosch et al. (2007) in the MZ.

7 Summary and conclusions

We have used ray tracing to study the propagation of O mode high frequency radio waves in a plane stratified ionosphere modified by pump-induced or natural kilometre-scale field aligned density depletions, or ducts, with special attention to transmission through the radio window.

The ducts were shown to shift the position of the radio window, or to introduce radio windows at entirely new locations by guiding the rays into the so-called L mode, which allows them to be efficiently transmitted. In a simplified model excluding absorption, we estimated the wave electric field strength perpendicular to the magnetic field at altitudes which are otherwise only accessible to rays at the critical angle. This field could excite upper hybrid waves on small scale density perturbations.

By plotting the wave field as a function of duct position, we also showed that the effects of transmission and focussing combine to give stronger fields in some directions, notably at angles close to the MZ. The results could therefore have implications for the MZ effect.

Acknowledgements. The authors gratefully acknowledge Anders Västberg for discussions, Anders Tjulin for the script used to produce Fig. 1, and the Swedish Research Council for financial support. We also wish to thank Todd Pedersen for valuable comments and suggestions during the review process.

Topical Editor K. Kauristie thanks M. Kosch and another anonymous referee for their help in evaluating this paper.

References

Bowman, G. G.: Triple splitting with the F2-region of the ionosphere at high and mid-latitudes, Planet. Space Sci., 2, 214–218, doi:10.1016/0032-0633(60)90018-0, http://www.sciencedirect.com/science/article/B6V6T-46YSK6R-1T/2/5f2b0bb21555498e339df29e723ae971, 1960.

Budden, K. G.: Radio Waves in the Ionosphere, Cambridge University Press, Cambridge, 1961.

Budden, K. G.: The theory of radio windows in the ionosphere and magnetosphere, J. Atmos. Terr. Phys., 42, 287–298, 1980.

Budden, K. G.: The propagation of radio waves, Cambridge, London, 1985.

Dysthe, K. B., Mjølhus, E., Pécseli, H., and Rypdal, K.: Thermal cavitons, Physica Scripta, T2/2, 548–559, 1982.

Ellis, G. R.: The Z propagation hole in the ionosphere, J. Atmos. Terr. Phys., 8, 43–54, 1956.

Farley, D. T., LaHoz, C., and Fejer, B. G.: Studies of the self-focusing instability at Arecibo, J. Geophys. Res., 88, 2093–2102, 1983.

Isham, B., Rietveld, M. T., Hagfors, T., Hoz, C. L., Mishin, E., Kofman, W., Leyser, T. B., and van Eyken, A. P.: Aspect angle dependence of HF enhanced incoherent backscatter, Adv. Space Res., 24, 1003–1006, 1999.

Kelley, M. C., Arce, T. L., Salowey, J., Sulzer, M., Armstrong, W. T., Carter, M., and Duncan, L.: Density depletions at the 10-m scale induced by the Arecibo heater, J. Geophys. Res., 100, 17367–17376, 1995.

Kosch, M. J., Rietveld, M. T., Senior, A., McCrea, I. W., Kavanagh, A. J., Isham, B., and Honary, F.: Novel artificial optical annular structures in the high latitude ionosphere over EISCAT, Geophys. Res. Lett., 31, L12805, doi:10.1029/2004GL019713, 2004.

Kosch, M. J., Pedersen, T., Mishin, E., Starks, M., Gerken-Kendall, E., Sentman, D., Oyama, S., and Watkins, B.: Temporal evolution of pump beam self-focusing at the High-Frequency Active Auroral Research Program, J. Geophys. Res., 112, A08304, doi:10.1029/2007JA012264, 2007.

Leyser, T. B. and Nordblad, E.: Self-focused radio frequency L wave pumping of localized upper hybrid oscillations in high-latitude ionospheric plasma, Geophys. Res. Lett., 36, L24105, doi:doi:10.1029/2009GL041438, 2009.

Mishin, E., Hagfors, T., and Isham, B.: A generation mechanism for topside enhanced incoherent backscatter during high frequency modification experiments in Tromsø, Geophys. Res. Lett., 28, 479–482, 2001.

Mjølhus, E.: On linear conversion in a magnetized plasma, Radio Sci., 25, 1321–1339, 1990.

Mjølhus, E.: Theoretical model for long time stimulated electromagnetic emission generation in ionospheric radio modification experiments, J. Geophys. Res., 103, 14711–14729, 1998.

Papagiannis, M. D. and Miller, D. L.: Ray-tracing of the Z-mode in a tilted layer ionosphere, J. Atmos. Terr. Phys., 31, 155–163, 1969.

Pedersen, T., Esposito, R., Starks, M., and McCarrick, M.: Quantitative determination of HF radio-induced optical emission production efficiency at high latitudes, J. Geophys. Res., 113, A11316, doi:10.1029/2008JA013502, 2008.

Rietveld, M. T., Kosch, M. J., Blagoveshchenskaya, N. F., Kornienko, V. A., Leyser, T. B., and Yeoman, T. K.: Ionospheric electron heating, optical emissions, and striations induced by powerful HF radio waves at high latitudes: Aspect angle dependence, J. Geophys. Res., 108, 1141, doi:10.1029/2002JA009543, 2003.

Starks, M. J.: Effects of HF heater-produced ionospheric depletions on the ducting of VLF transmissions: A ray tracing study, J. Geophys. Res., 107, 1336, doi:doi:10.1029/2001JA009197, 2002.

Swanson, D. G.: Plasma Waves, 2nd Ed., IOP Publishing, London, 2003.